ADVANCED FUNCTIONAL MATERIALS
www.afm-journal.de

Structural Confinement toward Giant Enhancement of Red Emission in Mn^{2+}-Based Phosphors

Zhichao Zhang, Chonggeng Ma, Romain Gautier, Maxim S. Molokeev, Quanlin Liu, and Zhiguo Xia**

Structural confinement effect on a pair of Eu^{2+} and Mn^{2+} optical centers is developed to realize the greatly enhanced red emission attributed to the $^4T_1(^4G)$–$^6A_1(^6S)$ transition of Mn^{2+} ions. $Sr_9Mn_{1.26(2)}Li_{0.24(2)}(PO_{4-\delta})_7$, when it is doped with Eu^{2+}, emerges as a new red-emitting phosphor, and the intensity dependence of such a red emission on the trace amounts of Eu^{2+} doping is quantitatively analyzed with a combined experimental and theoretical methods. The modeling result confirms the validity of this proposed design strategy, and the intrinsic high-efficient Eu^{2+}–Mn^{2+} energy transfer process can be elucidated by the structural confinement effect featured as some Sr (Eu) close to Mn atoms. The results can initiate the exploration of Mn^{2+}-based red phosphors for pc-white light-emitting diodes applications, and such a strategy can be easily expanded to other systems, thus opening a new perspective for the development of luminescence materials.

1. Introduction

The solid-state lighting technology originating from the phosphor-converted white light-emitting diodes (pc-WLEDs) penetrated deeply into various home/lifestyle products including the indoor/outdoor illumination and backlight units in modern liquid-crystal display (LCD) applications.[1] Key materials discoveries represented by the broad-band yellow-emitting $Y_{3-x}Gd_xAl_{5-y}Ga_yO_{12}:Ce^{3+}$ phosphors combined with the blue-emitting semiconductor InGaN chip, have prompted the development of lighting, displays and other applications.[2] However, one of the remaining challenges is to further improve the color rendition and optical quality of illumination-grade light sources.[3] Amongst, the development of red-emitting phosphors provides new opportunities for fabricating pc-WLEDs with both high color rendering index and high luminous efficacy.[4] At present, plenty of red-emitting phosphor materials have been discovered based on versatile structural models, among them, Eu^{2+}-doped nitrides, such as, $(Ba,Sr)_2Si_5N_8:Eu^{2+}$ and $(Ca,Sr)SiAlN_3:Eu^{2+}$, as well as Mn^{4+}-doped fluoride represented by $K_2SiF_6:Mn^{4+}$, have drew much attentions.[2a,5] It is clear that the design of new red emitter is a key challenge for the emerging applications of future phosphors.[6]

A useful approach, also called as the mineral-inspired prototype evolution and new phase construction strategy, has been successfully adopted to construct the new phases acting as the phosphor hosts.[2,7] As an example discussed herein, β-$Ca_3(PO_4)_2$-type mineral structure is capable of such a design principle toward new phosphor systems owing to the possibility for heterovalent substitution of cations and multivariate structural types.[2a,8] This phase provides five crystallographic cationic position with opportunities for heterovalent substitution and close interactions between cations.[9] Moreover, a valid approach is to target an efficient energy transfer (ET) for color-tunable phosphors, so that the ET process can be easily realized in the multiple sites of the β-$Ca_3(PO_4)_2$-type compounds.[10] Inspired by the above reasons, we discovered a new β-$Ca_3(PO_4)_2$-type compound in which Eu^{2+}–Mn^{2+} ET in the local confinement space has been found and verified.

Mn^{2+} based β-$Ca_3(PO_4)_2$-type compound with the nominal chemical formula of $Sr_9MnLi(PO_4)_7$ has been designed, and the crystal structure was resolved by the single crystal X-ray diffraction method based on the microcrystal samples. And it is

Z. C. Zhang, Prof. Q. L. Liu, Prof. Z. G. Xia
The Beijing Municipal Key Laboratory of New Energy Materials and Technologies
School of Materials Sciences and Engineering
University of Science and Technology Beijing
Beijing 100083, P. R. China
E-mail: xiazg@ustb.edu.cn

Prof. C. G. Ma
College of Sciences
Chongqing University of Posts and Telecommunications
Chongqing 400065, P. R. China
E-mail: cgma.ustc@gmail.com

Prof. R. Gautier
Institut des Matériaux Jean Rouxel (IMN)
Université de Nantes
CNRS
2 rue de la Houssinière, BP 32229, 44322 Nantes, Cedex 03, France

Prof. M. S. Molokeev
Laboratory of Crystal Physics
Kirensky Institute of Physics
Federal Research Center KSC SB RAS
Krasnoyarsk 660036, Russia

Prof. M. S. Molokeev
Department of Engineering Physics and Radioelectronics
Siberian Federal University
Krasnoyarsk 660041, Russia

Prof. M. S. Molokeev
Department of Physics
Far Eastern State Transport University
Khabarovsk 680021, Russia

The ORCID identification number(s) for the author(s) of this article can be found under https://doi.org/10.1002/adfm.201804150.

DOI: 10.1002/adfm.201804150

worth mentioning that the intensity of Mn^{2+} emission centers in this compound has been increased 159 times with the introduction of the trace amount of Eu^{2+} doping, which is ascribed to the highly efficient Eu^{2+}–Mn^{2+} ET probability rate. The excitation and emission spectra of pure and Eu^{2+}-doped samples were analyzed in the framework of the crystal field (CF) theory. On the basis of the obtained CF energy level diagrams of Eu^{2+} and Mn^{2+} ions, various pumping kinetic processes to the luminescent $^4T_1(^4G)$ energy level of Mn^{2+} ions were discussed by means of spectroscopic modeling, and the dependence of the relative luminescence intensity of Eu^{2+}-doped samples on the Eu^{2+} doping concentration was calculated and compared with the measurement. The results verify that the structural confinement effect application should be a power strategy to enhance the red emission of Mn^{2+} ions and discover new phosphors for pc-WLEDs.

2. Results and Discussion

The designed compound with the targeted chemical formula $Sr_9MnLi(PO_4)_7$ is hypothetical and derived from β-$Ca_3(PO_4)_2$-type phase, which is actually not included in any structural data base. Accordingly, this compound was synthesized through the traditional solid-state reaction yielding homogeneous powder particles. In **Figure 1**a, it is seen that the sample is composed by individual grains and this is very strange because, commonly, the samples formed by solid state synthesis contain agglomerated grains. It can be observed from the scanning electron microscope (SEM) measurements that the particles are of relatively uniform morphology with smooth surface and their sizes are about 20 µm. A typical microcrystal particle (Figure 1b) was selected to perform the elemental mapping analysis. The overlap and individual element Sr, Mn, P, and O have been demonstrated in Figure 1c–g, and all the elements are homogeneously distributed in the particles. The images of phosphor particles were checked by fluorescent microscopy, as shown in Figure 1h for optical microscope mode and Figure 1i for fluorescence imaging mode, respectively. The microcrystals demonstrated high crystallinity and bright red emission upon 380 nm UV illumination. The crystal structure of the compound was solved from the single crystal X-ray data of the single microparticle. The main information about the

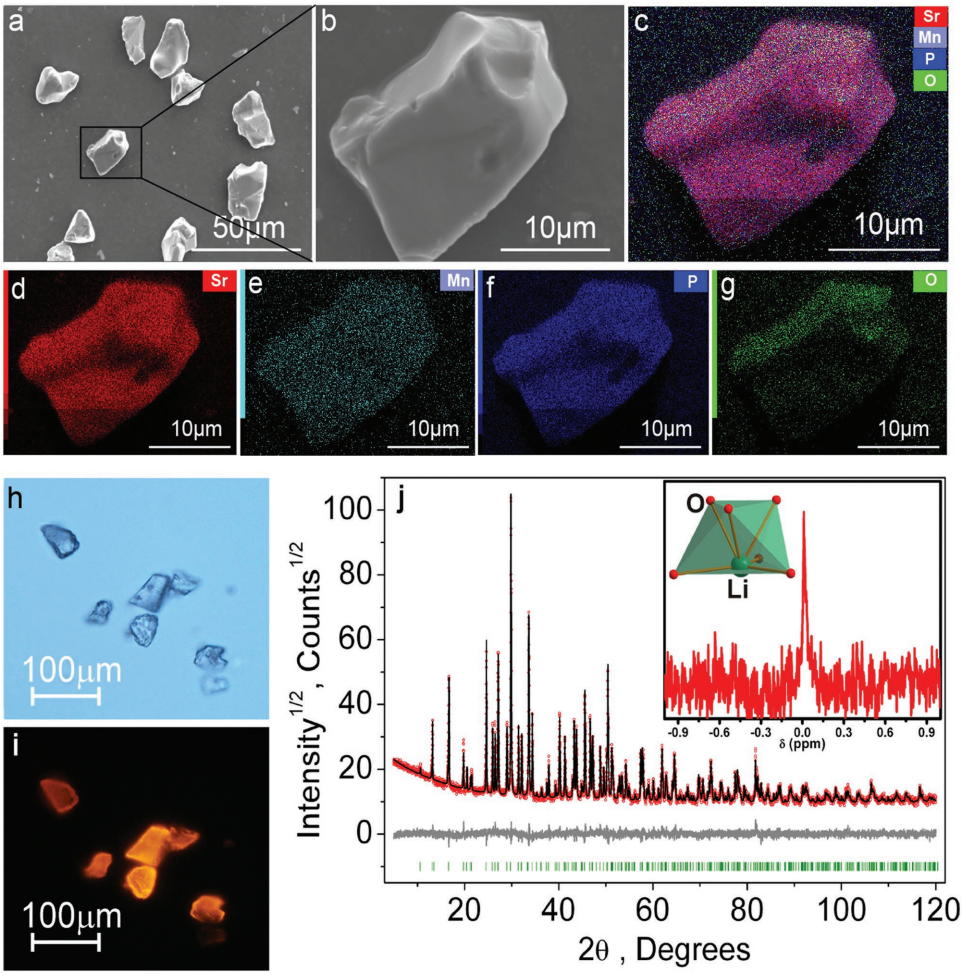

Figure 1. SEM images of targeted SMLPO:Eu^{2+} at a) low and b) high magnifications, and the corresponding EDS elemental mapping images for c) overlap elements, and the independent element d) Sr, e) Mn, f) P, and g) O. Microscopy images of the selected microcrystals in the h) daylight and i) upon 380 nm UV illumination. j) Rietveld refinement of powder pattern using structural model obtained from single crystal diffraction and the inset shows ^{6}Li MAS NMR spectrum and the coordination environment.

crystallographic data collection and refinement was reported in Table S1 in the Supporting Information. The structure of $Sr_9Fe_{1.5}(PO_4)_7$ was taken as a starting model for refinement considering the similarity of the average ionic radii of the substituent Mn^{2+}/Li^+ and the original Fe^{2+} in the host, also including the same disordering of structural elements.[11] The occupancies of Sr2 and Sr3 sites were refined with a constraint of occ(Sr2) + occ(Sr3) = 0.5 according to $Sr_9Fe_{1.5}(PO_4)_7$ model. The Fe^{2+} ions were replaced by Mn^{2+}/Li^+ ions and the occupancies were allowed to be refined. The Mn^{2+} and Li^+ atoms were refined with the same coordinates and equal thermal parameters. The thermal parameters of all atoms besides disordered ions (Sr2, Sr3, P1, O1, O2) were refined anisotropically. It was found that only one (Mn1) site from two independent Mn sites (Mn1, Mn2) in the asymmetric unit has noticeable value of Li occupation. Therefore, at the final stage of refinement, the Li occupation in the Mn2 site was fixed to be zero (Table S2, Supporting Information). It should be noted that the replacement of Mn^{2+} by Li^+ leads to small charge disbalance about –0.24 e, and, respectively, the existence of O^{2-} vacancy was assumed which cannot be refined. The chemical formula from the final refinement can be written as $Sr_9Mn_{1.26(2)}Li_{0.24(2)}(PO_{4-\delta})_7$, abbreviated as SMLPO hereafter, and the crystallographic information file (CIF) of this new phase is presented in the Supporting Information. One can see that Li really penetrates into the host, moreover, the ^{6}Li MAS NMR spectrum from grounded crystals shown in the inset of Figure 1j demonstrated the chemical shift, δ = 0.02 ppm, which indicated that Li entered the lattice and formed six-coordinated LiO_6 octahedron.[12] Thus, the Li incorporation was further confirmed. Accordingly, Rietveld refinement of powder pattern, which was obtained by X-ray diffraction (XRD) of ground single crystals, showed that the bulk material is of pure phase (Figure 1j). The as-obtained SMLPO phase crystallizes as a trigonal structure with space group *R-3m*. The unit cell parameters were determined to be a = 10.652 (1) Å, b = 10.652 (1) Å, c = 19.699 (3) Å, V = 1935.7 (6) Å^3.

Figure 2a,b represents the details of SMPLO crystal structure refined from single crystal X-ray diffraction. It should be noted that there are two Mn sites in the asymmetric unit, one of them, Mn2, is ordered and forms regular octahedron, however, Mn1 site contains Mn^{2+}, Li^+ ions and vacancy which are statistically disordered over crystal (Figure 2b). The Mn1/Li1/Vacancy site has complex form of polyhedron because it shares the face with $P1O_4$ tetrahedron which is disordered over three positions (Figure 2a). Crystal structure analysis revealed the short distances $d_{(Sr2/3\text{-}Mn1)}$ = 2.402–3.788 Å (Figure 2a). However, the small occupancy values of occ(Sr3) = 0.178 (9), occ(Sr2) = 0.319 (9), and occ(Mn1) = 0.13 (1) imply that, in the case of statistical disordering with random ion distribution over space, such bond lengths hardly can be observed. Taking into account the repulsive character of Mn^{2+} and Sr^{2+} ions one can suggest almost zero probability of such situation. Only in the case of dynamical disordering of Sr^{2+} ions, in the hypothetical situation when Sr^{2+} jumps from one position to another one with high frequency, this can lead to such short Sr—Mn bond lengths for

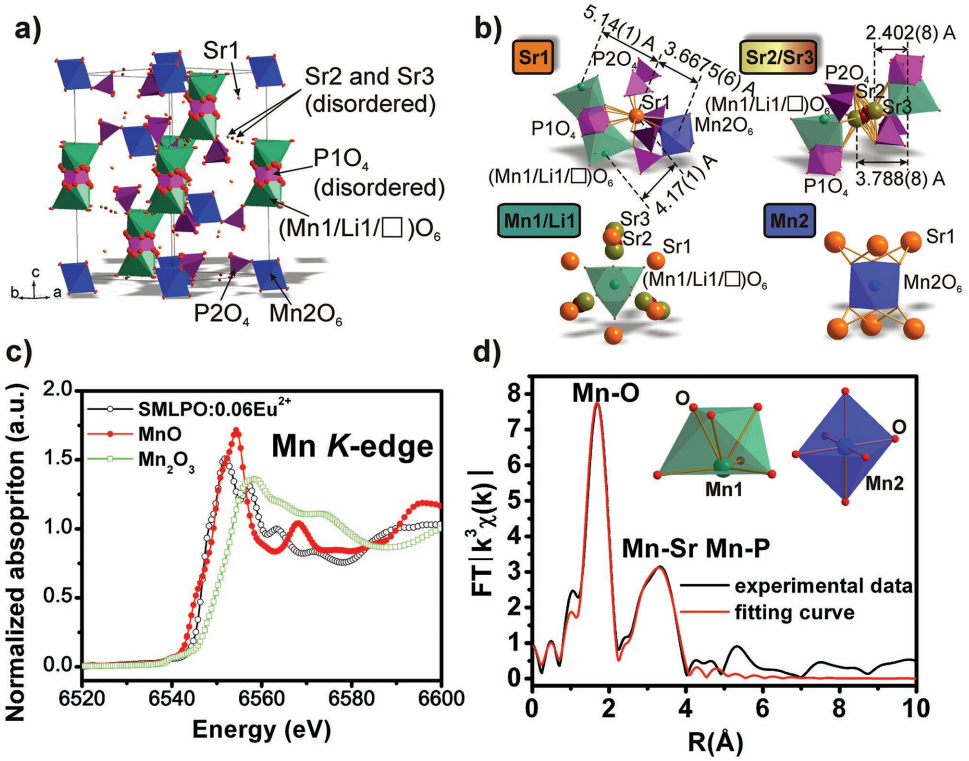

Figure 2. a) Crystal structure of SMPLO refined from single crystal diffraction, and several structural elements are disordered: Sr2, Sr3, $P1O_4$, and Mn1/Li1/Vacancy. b) Coordination diagram of Sr1, Sr2/Sr3, Mn1/Li1, and Mn2 sites by other structural elements. c) The normalized Mn K-edge XANES spectra of SMLPO:Eu^{2+} and the reference compounds of MnO and Mn_2O_3. d) Fourier transform of the EXAFS spectra of SMLPO:Eu^{2+} fitting use a function of *R*.

short durations. This effect cannot be excluded because XRD measurements cannot distinguish static from dynamic disorder. In any case, the fully occupied Sr1 and Mn2 sites also have relatively short bond lengths $d_{(Sr1–Mn2)}$ = 3.6675–5.14 Å which would permit efficient ET discussed later. In order to further corroborate the crystal structure details, we adopted the X-ray absorption near-edge spectroscopy (XANES) and extended X-ray absorption fine structure (EXAFS) to provide electronic information and symmetry information for manganese in the SMLPO:Eu^{2+} compound. The Mn K-edge XANES spectra of SMLPO:0.06Eu^{2+} and reference samples MnO and Mn_2O_3 are given in Figure 2c. The pre-edge feature of the K-edge of manganese is located 15–20 eV before the main K-edge crest of manganese. A weak absorption peak at ≈6540 eV can be observed and it is attributed to the electric dipole forbidden transition from the 1s core levels to the empty 3d levels more or less 4p hybridized by the oxidation state and the ligand environment of the metal. By comparing a closeness of the Mn edge, the SMLPO:Eu^{2+} sample was similar to MnO reference sample when normalized absorption is equal to 0.75. This comparative analysis shows that the Mn valence in this compound is +2. Moreover, the Mn K-edge shape is highly dependent on the compound type. The shape, position, and size of the peak provide information on the nearest neighbors in the compound probed by the EXAFS measurements. The EXAFS spectrum of SMLPO:Eu^{2+}, as well as the Fourier transform *R* functions, are shown in Figure 2d. For the Mn—O, Mn—Sr, and Mn—P shells fit to the compound, the coordination number (*N*) is calculated to be 5.6, 12, and 3.6, respectively, which yields the approximate values of 6, 12, and 4, and further with the respective interionic distances 2.15, 3.76, and 3.47 Å, respectively. These values are also in agreement with the crystal structure refinement results mentioned above.

Figure 3a illustrate the photoluminescence excitation (PLE) and photoluminescence emission (PL) spectra of the neat SMLPO and SMLPO:0.06Eu^{2+} samples, respectively. In the PLE spectrum of SMLPO, it can be elucidated that the strong excitation band with maximum at 205 nm (A) should be due to the host absorption, whereas other weak bands appearing in the range from 300 to 500 nm via an intensity enlargement by 20 times can be attributed to the transitions from $^6A_1(^6S)$ to $^4T_2(^4G)$, $^4E(^4G)$ and $^4A_1(^4G)$, $^4T_2(^4D)$, $^4E(^4D)$, and $^4T_1(^4P)$ of the $3d^5$ configuration of Mn^{2+} ions by employing the Tanabe–Sugano energy level diagram for the $3d^5$ configuration of Mn^{2+} ion.[13] Since the observed 3d–3d transitions are both parity- and spin-forbidden, the intrinsic excitation of Mn^{2+} ions is very weak and inefficient, and the Eu^{2+} ions introduced as sensitizers improved significantly the PL emission. The PLE spectrum of SMLPO: 0.06Eu^{2+} exhibits the host absorption band A as well and two additional strong excitation bands with the maxima at 312 nm (B) and 355 nm (C), respectively. The latter two can be simply regarded as the transitions of Eu^{2+} ions from the $4f^7$ ground multiplet $^8S_{7/2}$ to those $4f^65d^1$ states with the first and second 5d CF components, respectively. A more

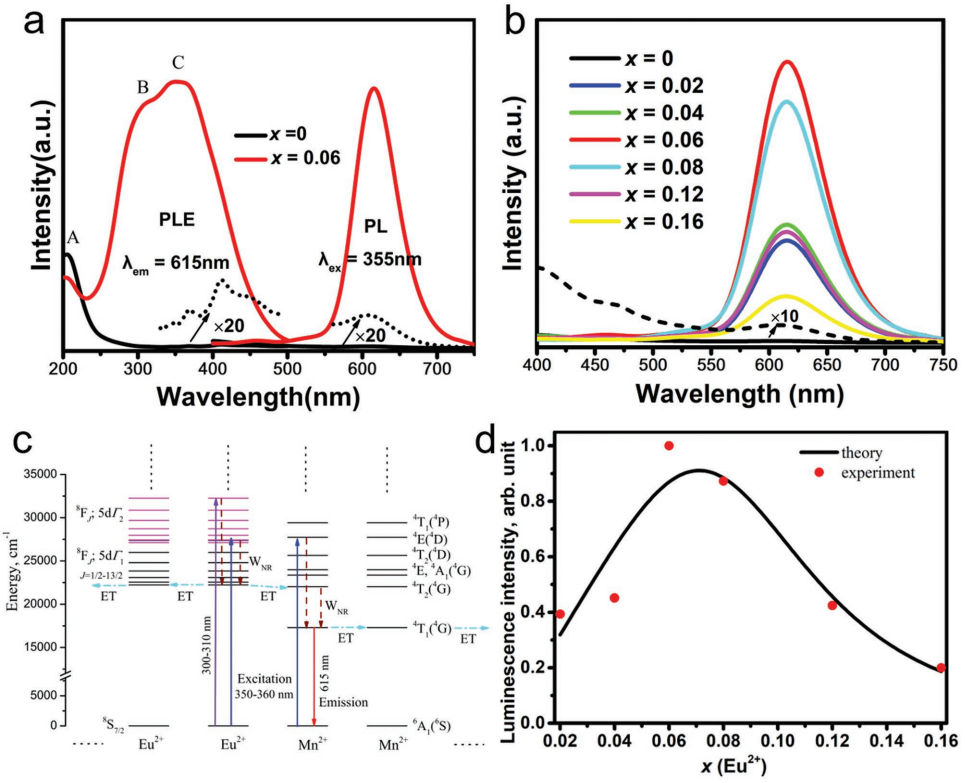

Figure 3. a) Photoluminescence excitation and emission, spectra of SMLPO:xEu^{2+} phosphors, with $x = 0$ (black line the enlarged dot-ted line), $x = 0.06$ (red line). b) PL spectra of a series of SMLPO:xEu^{2+} (x = 0–0.16 mol) phosphor under 355 nm excitation. c) Schematic diagram for luminescence kinetics of pure and Eu^{2+}-doped SMLPO. d) Calculated and measured dependence of the relative luminescence intensities of the Eu^{2+}-doped SMLPO samples on the concentration of Eu^{2+} ions.

accurate assignment for them can be made based on our recently proposed $4f^65d^1$ energy level scheme of Eu^{2+} ion using the notation $|(4f^67F,s_d)^8F_j; 5d\Gamma i>$ ($i = 1$ and 2; $J = 1/2,...,13/2$),[7b] as shown in Figure 3c. The PL spectra of both SMLPO and SMLPO: $0.06Eu^{2+}$ shows one broad red emission peak at about 615 nm originating from the 3d–3d transition from $^4T_1(^4G)$ to $^6A_1(^6S)$ of Mn^{2+} ions. One can also find that such a red emission can be greatly enhanced after doping Eu^{2+} ions. Figure 3b shows the PL spectra of SMLPO:xEu^{2+} samples ($x = 0.02$–0.16) excited at 355 nm, and the PL intensity dependence on the concentration of Eu^{2+} ions is depicted in Figure 3d. It can be clearly seen that the PL intensity increases sharply with the introduction of Eu^{2+} ions, and reaches the maximum ($x = 0.06$) with being 159 times stronger than the pure host case. Such increase of the PL intensity can be explained as the fact of the ET process with high efficiency between Eu^{2+} and Mn^{2+} ions, whereas the following quenching behavior should be caused by the increasing energy loss during the excitation energy migration process among Eu^{2+} ions with increasing concentration.[14] The PL decay curves of a series of SMLPO:xEu^{2+} phosphors ($x = 0$–0.16) with monitoring the emission of Mn^{2+} ions at 615 nm and the excitation of Eu^{2+} ions at 355 nm were measured, as shown in Figure S1 in the Supporting Information. None of the decay curves shows a singly-exponential law because of the multicenter character of Mn^{2+} ions in the host lattice and the existence of delays in the Eu–Mn ET processes probably due to the energy retrapping by other Eu^{2+} ions or defects. Therefore, the average lifetime characterized by the formula proposed in Ref. [15] should be a good descriptor for the nonexponential decay cases. The dependence of the calculated average lifetime on the concentration of Eu^{2+} ions is given in Figure S1 (Supporting Information) and it looks similar as the PL dependence in Figure 3d. The observed dependences suggest that a piling up effect on the occupation number of the $^4T_1(^4G)$ state of Mn^{2+} ions caused by the Eu–Mn ET processes form a competition with the spontaneously radiative process to the ground state $^6A_1(^6S)$ of Mn^{2+} ions, and, then, much stronger the Eu–Mn ET processes, much longer the average lifetime. Moreover, the external and internal quantum efficiency of SMLPO:$0.06Eu^{2+}$ phosphors are 16.84% and 29.97%, respectively, at room temperature, and the measurement details are shown in the Supporting Information.

In order to understand the role of the structural confinement effect in the enhancement of red emission intensity of Mn^{2+} ions, we combined the two proposed energy level diagrams for Eu^{2+} and Mn^{2+} ions in SMLPO to obtain the description of various pumping kinetic processes to the luminescent $^4T_1(^4G)$ energy level of Mn^{2+} ions, as shown in Figure 3c. By inspecting Figure 3c, one can find that the structural confinement effect acting on a pair of cationic optical centers should be mainly responsible for tuning the metal-to-metal ET probability rates, such as those from Eu^{2+} to Mn^{2+} ions in SMLPO. Following the classical Dexter ET theory,[16] we estimated the order of magnitude of the Eu–Eu, Eu–Mn, and Mn–Mn ET probability rates in SMLPO with respect to the reference system $Ca_2Sr(PO_4)_2$:$0.04Eu^{2+}$, $0.08Mn^{2+}$ with the similar structural form[17] and collected them into Table S3 in the Supporting Information. From Table S3 (Supporting Information), one can see that the structural confinement effect, due to the short distance between the Sr1 and Mn2 sites, results in much stronger Mn–Mn and Eu–Mn ET probability rates relative to that in the reference system and can further suppress the luminescence of Eu^{2+} and Mn^{2+} ions. Although the Mn–Mn ET decreases the population of the luminescent $^4T_1(^4G)$ energy level of Mn^{2+} ions, the more high-efficient Eu–Mn ET process provides a very robust pumping behavior and therefore significantly enhances the red emission of Mn^{2+} ions, as confirmed by the experimental measurements and theoretical calculations (Supporting Information). In addition, the measured dependence of the luminescence intensities of the Eu^{2+}-doped samples on the Eu^{2+}-doping concentration was also modeled by extending the theoretical model above on the basis of considering the competition among the 5d–4f luminescence of Eu^{2+} ions and the Eu–Eu and Eu–Mn ETs. The calculated dependence given in Figure 3d shows a very good agreement with the experimental results and the related numerical simulation results given in Table S4 (Supporting Information) perfectly support the experimental fact that the 5d–4f luminescence of Eu^{2+} ions is too weak to be observed.

To further evaluate the application of SMLPO:Eu^{2+} as white LEDs phosphor, the position of the SMLPO: $0.06Eu^{2+}$ phosphor excited at 355 nm at the Commission Internationale de I'éclairage (CIE) chromaticity diagram was calculated and a digital photograph under 365 nm UV lamps is given (**Figure 4**a). As shown in the inset, the phosphor of SMLPO: Eu^{2+} shows bright red emission with the CIE coordinates of (0.5907, 0.3691). Hence, blue-emitting $BaMgAl_{10}O_{17}$:Eu^{2+}, green-emitting Ba_2SiO_4:Eu^{2+} and red-emitting SMLPO:$0.06Eu^{2+}$ were combined in UV-LEDs chips (365 nm) to fabricate a pc-LED device. The electroluminescence spectrum of the packaged w-LED lamp driven by 360 mA current is exhibited in Figure 4b, and the image of the fabricated device is shown in inset. The CIE color coordinates of the fabricated pc-LED are revealed as (0.350,0.342) and the lower correlated color temperature (CCT) value 4762 K indicate bright warm white light emitted from the device. The color rendering index value (R_a) is obtained reached 91.2. These results demonstrated that SMLPO: Eu^{2+} has a great potential to serve as phosphor of pc-LED.

3. Conclusion

In summary, we have utilized the mineral-inspired prototype evolution and new phase construction strategy, as well as the further composition design via chemical cosubstitution leading to new materials and optimized properties, proposed by our group.[2a] Thus, the novel red-emitting Mn^{2+}-based phosphor, $Sr_9Mn_{1.26}Li_{0.24}(PO_{4-\delta})_7$:$Eu^{2+}$, based on β-$Ca_3(PO_4)_2$-type structure model has been discovered. The red emission can be enormously enhanced with trace amounts of Eu^{2+} doping due to the intrinsic high-efficient Eu–Mn ET process. The structural analysis and spectroscopic modeling confirm that such high-efficient Eu–Mn ET is induced by a structural confinement effect. The concept of energy transfer in the local confinement space could initiate the exploration of Mn^{2+}-based red phosphors for pc-WLEDs applications, and such a strategy can be easily expanded to other systems, thus opening a new perspective for the development of luminescence materials.

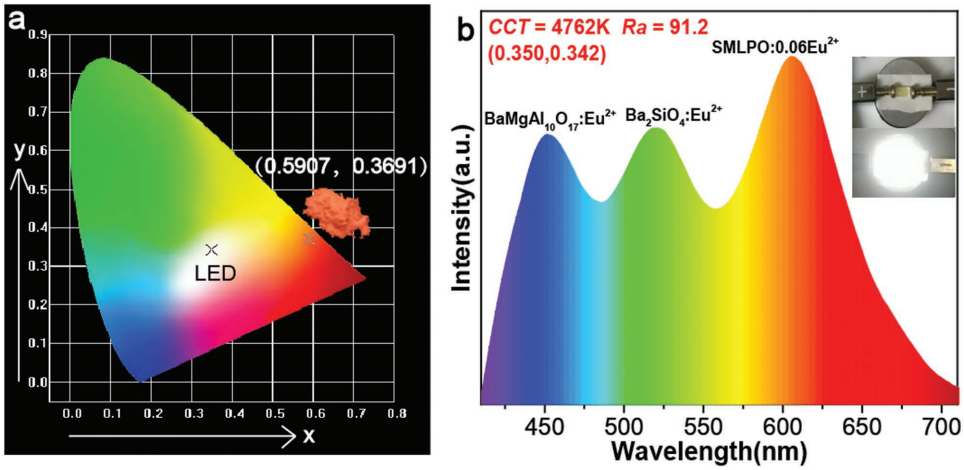

Figure 4. a) CIE chromaticity diagram of SMLPO: $0.06Eu^{2+}$ phosphor and white LEDs lamp and the digital photographs of SMLPO: $0.06Eu^{2+}$. b) EL spectrum of w-LED fabricated by blue $BaMgAl_{10}O_{17}:Eu^{2+}$, green $Ba_2SiO_4:Eu^{2+}$, and red SMLPO: $0.06Eu^{2+}$ on a UV-LED chip (λ = 365 nm), and the measured parameters are also shown.

4. Experimental Section

Materials and Preparation: Phosphors samples with the nominal chemical compositions of $Sr_9MnLi(PO_4)_7:xEu^{2+}$ were synthesized by a high temperature solid-state reaction method. The raw materials were $SrCO_3$ (99.99%, Sinopharm Chemical Reagent Co., Ltd), $NH_4H_2PO_4$ (99.99%, Sinopharm Chemical Reagent Co., Ltd), $MnCO_3$ (99.99%, Sinopharm Chemical Reagent Co., Ltd), Li_2CO_3 (99.99%, Sinopharm Chemical Reagent Co., Ltd), and Eu_2O_3 (99.99%, Aladdin Chemistry Co., Ltd). The raw materials were mixed by grinding in an agate mortar with a given stoichiometric ratio. Mixtures were then shifted to the crucible and preheated at 700 °C for 3 h. After being ground, the powder mixtures were sintered again at 1300 °C for 4 h under a reducing atmosphere of CO. After firing, the samples were cooled to room temperature in the furnace and then the final product was obtained in powder form with small microcrystals showing red luminescence after excitation with a 365 nm UV lamp. The powder products were used for the structural and spectral analysis.

Characterization: To determine the elemental composition, distribution, and the morphology of the obtained products, a JEOL JSM 6510 SEM equipped with an energy disperse spectrum (EDS) detector was used to check the ground samples. The photographs of microcrystal particle were obtained by an optical microscope equipped with fluorescence imaging system (Nikon Eclipse LV100ND), and the 380 nm illumination and Nikon DS-Qi2 CCD camera were also used. The single crystal X-ray diffraction data of the selected microcrystal sample were collected on a Bruker D8-Venture single crystal X-ray diffractometer equipped with a Turbo X-ray Source (Mo–Kα radiation, λ = 0.71073 Å) adopting the direct drive rotating anode technique. Crystal structure solving and Rietveld refinements were performed by using TOPAS 4.2 software. The X-ray data from the crystal were measured for the exposure time of 10 s on each frame. Each new frame was obtained by crystal rotation along ω-axis by 0.5° at the fixed φ angle. The ω value was increased from 0° to 182°. The 364 frames were measured at each fixed φ equal to 0°, 120°, and 240°. After that, the program APEXII from Bruker integrated the reflection intensities. Space group *R*-3*m* was defined by the analysis of extinction rules and intensity statistics obtained from all reflections. The multiscan absorption correction of reflection intensities was performed by APEXII software. Then, the intensities of equivalent reflections were averaged. The structure refinement was carried out by least-square minimization in SHELXL 2014/7. 6Li solid-state nuclear magnetic resonance (NMR) spectra were obtained on a solid-state Bruker 400WB AVANCE 3 at 16 kHz. The X-ray absorption near-edge structure (XANES) spectra were recorded on the beam line of 1W1B at Beijing Synchrotron Radiation Facility. All spectra of XANES were normalized to a unity step height in the absorption coefficient from well below to well above the edges. Standard oxide powders, MnO and Mn_2O_3, were used for energy calibration and for comparing different electronic valence states. The photoluminescence emission (PL) and photoluminescence excitation (PLE) spectra were recorded by a fluorescence spectrophotometer (F-4600, HITACHI, Japan) equipped with a photomultiplier tube operating at 400 V and a 150 W Xe lamp as the excitation source. The luminescence decay curves were measured by the FLS920 fluorescence spectrophotometer (Edinburgh Instruments Ltd., U.K.).

White-Light LED Lamps Fabrication: White LED lamps were fabricated by integrating a mixture of transparent silicone resin and phosphors blend of blue-emitting $BaMgAl_{10}O_{17}:Eu^{2+}$, green-emitting $Ba_2SiO_4:Eu^{2+}$ commodity and orange-red-emitting $Sr_9Mn_{1.26(2)}Li_{0.24(2)}(PO_{4-\delta})_7:Eu^{2+}$ on an 365 nm UV chip. Optical properties, including the electroluminescence (EL) spectrum, color temperature (CCT), color rendering index (R_a), and CIE color coordinates of the LEDs, were characterized using a PMS-80 Plus UV–vis–near IR Spectrophotocolorimeter system.

Computational Methodology: The PLE and PL spectra of Mn^{2+} and Eu^{2+} ions in SMPLO were analyzed for the construction of the corresponding electronic energy level diagrams by employing the combination of the exchange charge model[18] describing the crystal-field effect felt by dopants and the simple model[19] for f–d transitions of lanthanide ions. The luminescence kinetic processes were described by means of the spectroscopic modeling including the Einstein absorption coefficient and the spontaneous emission transition probability rate in order to evaluate the luminescence enhancement times after doping Eu^{2+} ions. The Eu–Mn, Mn–Mn, and Eu–Eu energy transfer probability rates in SMPLO were estimated in the framework of the energy transfer theory of Dexter[16] and further fed into modeling the dependence of the luminescence intensities of the Eu^{2+}-doped samples on the doping concentration. More details about the theoretical background used in the present work can be found in the Supporting Information.

Supporting Information

Supporting Information is available from the Wiley Online Library or from the author.

Acknowledgements

The present work was supported by the National Natural Science Foundation of China (Grants 51722202, 91622125, and 51572023), Natural

Science Foundations of Beijing (2172036), and by Russian Foundation for Basic Research according to the research project 17-52-53031, and by the French National Agency for Research (ANR Young Researchers, ANR-16-CE08-0003-01, Combi-SSL project). C.-G.M. thanks supports from China Scholarship Council (CSC File No. 201607845015) and Wenfeng High-end Talents Project of CQUPT (Grant No. W2016-01). The authors would like thank Dr. Shuao Wang, Professor of Soochow University, for supplying the single crystal data collection.

Conflict of Interest

The authors declare no conflict of interest.

Keywords

phosphor, photoluminescence, structural confinement

Received: June 15, 2018
Revised: July 31, 2018
Published online: August 28, 2018

[1] a) P. Pust, P. J. Schmidt, W. Schnick, *Nat. Mater.* **2015**, *14*, 454; b) G. G. Li, Y. Tian, Y. Zhao, J. Lin, *Chem. Soc. Rev.* **2015**, *44*, 8688.
[2] a) Z. G. Xia, Q. L. Liu, *Prog. Mater. Sci.* **2016**, *84*, 59; b) Z. G. Xia, A. Meijerink, *Chem. Soc. Rev.* **2017**, *46*, 275.
[3] P. Pust, V. Weiler, C. Hecht, A. Tucks, A. S. Wochnik, A. K. Henss, D. Wiechert, C. Scheu, P. J. Schmidt, W. Schnick, *Nat. Mater.* **2014**, *13*, 891.
[4] R. Gautier, X. Y. Li, Z. G. Xia, F. Massuyeau, *J. Am. Chem. Soc.* **2017**, *139*, 1436.
[5] a) X. Qin, X. W. Liu, W. Huang, M. Bettinelli, X. G. Liu, *Chem. Rev.* **2017**, *117*, 4488; b) Z. G. Xia, Z. H. Xu, M. Y. Chen, Q. L. Liu, *Dalton Trans.* **2016**, *45*, 11214.
[6] L. Wang, R. J. Xie, T. Suehiro, T. Takeda, N. Hirosaki, *Chem. Rev.* **2018**, *118*, 1951.
[7] a) J. W. Qiao, L. X. Ning, M. S. Molokeev, Y. C. Chuang, Q. L. Liu, Z. G. Xia, *J. Am. Chem. Soc.* **2018**, *140*, 9730; b) Z. G. Xia, C.-G. Ma, M. S. Molokeev, Q. L. Liu, K. Rickert, K. R. Poeppelmeier, *J. Am. Chem. Soc.* **2015**, *137*, 12494.
[8] a) B. I. Lazoryak, A. A. Belik, R. N. Kotov, I. A. Leonidov, E. B. Mitberg, V. V. Karelina, D. G. Kellerman, S. Y. Stefanovich, A. K. Avetisov, *Chem. Mater.* **2003**, *15*, 625; b) H. P. Ji, Z. H. Huang, Z. G. Xia, M. S. Molokeev, V. V. Atuchin, S. F. Huang, *Inorg. Chem.* **2014**, *53*, 11119; c) P. Nandha Kumar, J. M. Ferreira, S. Kannan, *Inorg. Chem.* **2017**, *56*, 1289.
[9] M. Y. Chen, Z. G. Xia, M. S. Molokeev, T. Wang, Q. L. Liu, *Chem. Mater.* **2017**, *29*, 1430.
[10] a) M. M. Shang, C. X. Li, J. Lin, *Chem. Soc. Rev.* **2014**, *43*, 1372; b) J. Zhou, Q. Liu, Z. Xia, *J. Mater. Chem. C* **2018**, *6*, 4371.
[11] A. A. Belik, B. I. Lazoryak, K. V. Pokholok, T. P. Terekhina, I. A. Leonidov, E. B. Mitberg, V. V. Karelina, D. G. Kellerman, *J. Solid State Chem.* **2001**, *162*, 113.
[12] A. B. Santibáñez-Mendieta, C. Didier, K. K. Inglis, A. J. Corkett, M. J. Pitcher, M. Zanella, J. F. Shin, L. M. Daniels, A. Rakhmatullin, M. Li, *Chem. Mater.* **2016**, *28*, 7833.
[13] S. Sugano, Y. Tanabe, H. Kamimura, *Multiplets of Transition-Metal Ions in Crystals*, Academic Press, New York, USA **1970**.
[14] Z. G. Xia, Y. Y. Zhang, M. S. Molokeev, V. V. Atuchin, *J. Phys. Chem. C* **2013**, *117*, 20847.
[15] X. F. Liu, Y. Teng, Y. X. Zhuang, J. H. Xie, Y. B. Qiao, G. P. Dong, D. P. Chen, J. R. Qiu, *Opt. Lett.* **2009**, *34*, 3565.
[16] D. Dexter, *Solid State Phys.* **1958**, *6*, 353.
[17] Y. Chen, Y. Li, J. Wang, M. M. Wu, C. X. Wang, *J. Phys. Chem. C* **2014**, *118*, 12494.
[18] B. Z. Malkin, in *Crystal field and Electron–Phonon Interaction in Rare-Earth Ionic Paramagnets*, Vol. *21*, (Eds: A. A. Kaplyanskii, R. M. Macfarlane), North-Holland Publishing Company, Elsevier, Amsterdam **1987**, p. 51.
[19] C. Duan, M. Reid, *J. Solid State Chem.* **2003**, *171*, 299.

